SLAC-PUB-7845
June 1998

Active Millimeter-Wave Accelerator with Parallel Beams

David H. Whittum and Sami G. Tantawi

Stanford Linear Accelerator Center, Stanford University, Stanford, California 94309

We introduce a new concept for a miniature particle accelerator based on an active millimeter-wave circuit permitting a high gradient on nanosecond time-scales with much-reduced peak power and temperature cycling. We characterize the system using a transmission line model, and examine the transient features of operation as a coupled-cavity circuit including beam-loading. For illustration we consider an electromagnetic design for a seven-cell 91.4 GHz accelerator matched to standard waveguide, and a switch formed with a photoconductor in an H-plane tee geometry.

(submitted to Physical Review Letters)

Work supported by U.S. Department of Energy contract DE-AC03-76SF00515

Active Millimeter-Wave Accelerator with Parallel Beams

David H. Whittum and Sami G. Tantawi

Stanford Linear Accelerator Center, Stanford CA 94309

We introduce a new concept for a miniature particle accelerator based on an active millimeter-wave circuit permitting a high gradient on nanosecond time-scales with much-reduced peak power and temperature cycling. We characterize the system using a transmission line model, and examine the transient features of operation as a coupled-cavity circuit including beam-loading. For illustration we consider an electromagnetic design for a seven-cell 91.4 GHz accelerator matched to standard waveguide, and a switch formed with a photoconductor in an H-plane tee geometry.

PACS: 29.17+w, 07.57.Yb, 84.40.De, 72.40+w

The frontiers of high-energy physics today lie in the range of 0.5 TeV and beyond,[1] where size and cost are the first concerns, and physics-reach a distant second. Physics needs a new idea for acceleration, one that overcomes the limits on the electric field achievable in a pulsed microwave circuit, and this need has motivated a decade of research in advanced accelerator concepts.[2] The limits on electric field in conventional accelerators are field-emission, breakdown and cyclic fatigue due to Ohmic losses,[3] and these limits are fundamental to the conventional concept for two reasons: (1) microwave accelerators are *passive* devices, achieving large fields only by means of resonant external excitation over a *long* time scale of order the natural decrement time for fields due to wall losses,[4] and (2) they *combine* the function of resonant energy storage and acceleration in one structure. The technology of the high shunt impedance multi-cavity accelerator has been developed over many years, commencing with the cavity concepts of Hansen,[5] and evolving into machines of 100 m scale,[6] and later 3 km scale.[7] Prototyping for a 30 km machine is underway.[1]

In this work we set down a new concept for an accelerator, invoking a circuit that (1) is *active* and (2) *separates* the functions of energy storage and acceleration. As depicted schematically in Fig. 1, it consists of a primary transmission line coupled by means of fast switches to a series of parallel secondary transmission lines. Operation consists of three steps: (1) resonant filling of the primary line with mm-wave power P_1, provided by an external power source on the natural field decrement time scale of 10^{-8} s (2) switch closure on a time scale under 10^{-9} s (3) propagation of a sub-nanosecond burst of mm-waves down the secondary line, as electron bunches arrive in parallel. As seen in Fig.2, we implement the primary line as a standing wave cavity characterized by wall quality factor, Q_{w1}, external coupling factor, Q_{e1}, and angular resonance frequency ω. Total energy stored in the cavity for charging pulse-width t is

$$N_1 U_1 = \frac{2\beta}{1+\beta}\frac{\left(1-e^{-\tau_1}\right)^2}{\tau_1}\left(P_1 t\right), \tag{1}$$

with $T_1 = 2Q_{w1}/(1+\beta)\omega$, the loaded fill-time and $\beta = Q_{w1}/Q_{e1}$, the coupling parameter, and $\tau_1 = t/T_1$. The quantity U_1 is the energy available for discharge into each of the N_1 secondary lines after switch closure. Well-matched in the on-state, the primary cell produces a square wave with pulse length $T_p = 2w_1/V_{gp}$, where V_{gp} is the group velocity in the primary cell viewed as rectangular waveguide, and w_1 is the length of the primary cell in x. The peak power incident on the secondary line is $P_2(x=0) = U_1/T_p$, and is related to the group velocity for the secondary V_{g2}, and the energy stored in a secondary cell U_2 according to $P_2 = V_{g2}U_2/w_2$. The gradient G achievable in the secondary line may then be determined from

$$G^2 \approx \omega\left(\frac{U_2}{L}\right)\frac{1}{L}\left[\frac{R}{Q}\right], \tag{2}$$

where L is the width of one secondary cell, and $[R/Q]$ is determined from the geometry. The single-pulse temperature rise may be expressed in terms of pulse-width T_p as[3]

$$\Delta T_{\max} \approx \frac{0.84}{\sqrt{\kappa C}}\left(\frac{\delta}{\lambda}\right)\frac{G^2 T_p^{1/2}}{[R/Q]}\eta_g\eta_t . \tag{3}$$

For room-temperature copper the thermal conductivity is $\kappa = 401\ \mathrm{W/K-m}$, and the volume specific heat capacity is $C = 3.45\times10^6\ \mathrm{J/K-m^3}$. The conductivity of copper

$\sigma \approx 5.8 \times 10^7$ mho/m determines the skin-depth $\delta \approx 2.1\,\mu\text{m}\ f^{-1/2}(\text{GHz})$, with $f = \omega/2\pi$ the frequency. The quantity η_t depends on the waveform shape, with $\eta_t = 1$ for a square-wave. The quantity η_g depends on the cavity shape, with $\eta_g = 1$ for the geometry we will consider, a symmetric rectangular pillbox.

In the first approximation, both the primary cell, and the secondary cell are rectangular pillboxes, excited in the $\text{TE}_{10\text{m}}$ mode, with *m*=1 for the secondary cell, and, we will suppose, $m = 15$, for the primary cell. Such an idealized geometry permits explicit calculation of the circuit parameters Q_w and $[R/Q]$. We find

$$\frac{1}{Q_w} = 2\frac{R_s}{Z_0}\left\{\frac{1}{\theta} + \frac{\lambda^3}{4\pi}\left(\frac{1}{w_2^3} + \frac{1}{a^3}\right)\right\}, \tag{4}$$

$$\left[\frac{R}{Q}\right] = Z_0 \frac{4\lambda^2}{\pi^2 a w_2} \frac{\sin^2\left(\frac{\theta}{2}\right)}{\left(\frac{\theta}{2}\right)}, \tag{5}$$

where $\theta = \omega L/c$ is the transit angle, $\lambda = c/f$ is the free-space wavelength, c the speed of light, the surface resistance $R_s = 1/\sigma\delta \approx 8.3\text{m}\Omega\ f^{1/2}(\text{GHz})$, and $Z_0 \approx 376.7\,\Omega$. The cell depth is a, the width is w_2, and the transit-length is L as seen in Fig. 2. Minimum stored energy density on the primary line, U_1/L, favors maximum $[R/Q]/L$. However, too small a transit angle imples a low Q_w, and a thin and more fragile, structure. For simplicity we will optimize instead the stored energy per secondary line, maximizing $[R/Q]$. This requires $\theta \approx 133.6°$, $L = 0.371\lambda$ and $a = w_2 = \lambda/\sqrt{2}$ and gives $[R/Q] \approx 221.3\,\Omega$ and $Q_w \approx 2.6 \times 10^4 f^{-1/2}(\text{GHz})$.

For illustration we will consider $f = 91.392$ GHz (a harmonic for existing beamlines) for which the dimensions $a = w_2 = 2.32$ mm, $L = 1.22$ mm, and $Q_{w2} \approx 2.7 \times 10^3$ assuming a surface roughness much less than $\delta \approx 0.22\mu m$. The group velocity in the discharging primary line is $V_{gp}/c = 1/\sqrt{2}$, and $T_p = 2m/f \approx 0.33$ ns. The primary wall Q is $Q_{w1} \approx 3.6 \times 10^3$ with iris-loading, and $Q_{w1} \approx 9.9 \times 10^3$ without, and we will assume the latter. The natural decrement time is $2Q_{w1}/\omega \approx 34.6$ ns, and with critical coupling, the loaded fill-time is $T_1 \approx 17.3\,\mathrm{ns}$. For a gradient $G \approx 1\,\mathrm{GeV/m}$, pulsed temperature rise is $\Delta T_{\max} \approx 126$ K. For comparison, in a conventional accelerator circuit at W-Band the temperature rise would be $660\,\mathrm{K}$, and at X-Band the copper would melt in one pulse.

An unusual and intrinsic feature of this concept is dispersion of the waveform on the secondary line. We consider a secondary line designed for zero first-order dispersion, $\beta''(\omega_0) = 0$, where β is the wavenumber. The dispersing square-wave may then be expressed as an integral of the Airy function, and one can show that the minimum pulse length for maintenance of peak voltage is $T_p \geq 1.8(\beta''' x)^{1/3}$. To make this explicit, we adopt the periodic-line dispersion relation $\omega^2 = \omega_0^2(1-\kappa\cos\theta)$, where κ is the cell-to-cell coupling constant, and θ is the phase advance per cell, $\theta(\omega) \equiv \beta(\omega) w_2$, with w_2 the cell period. The group velocity is $\beta_g c = w_2 \kappa \omega_0^2 \sin\theta / 2\omega$. The condition for zero first order dispersion is $\tan\theta = 2^{1/2}\pi / \beta_g$ and this implies phase-advance near π/2, modulo π. Second-order dispersion is $(\theta''')^{1/3} \approx 2^{1/2}\pi / \beta_g \omega$. The constraint due to dispersion becomes $\beta_g \geq 1.3 N_2^{1/3} / N_c$, where the number of cycles in the pulse is $N_c = f\,T_p \approx 30$. Losses on the line may be compensated with tapering, and we employ $\beta_g' = -\omega / Q_{w2} c$ (a "constant-gradient" taper). In terms of $\Gamma = -w_2 \beta_g' / \beta_g(0)$, maintenance of the transient peaking voltage limits the number of secondary cells (beamlines),

$$N_2 \leq \frac{1}{\Gamma}\left\{1 - \frac{1}{\sqrt{1+2\Gamma\hat{N}_{\max}}}\right\}, \tag{6}$$

where $\hat{N}_{\max}^{1/3} \approx \beta_g(0) N_c / 1.3$. We will consider $\beta_g(0) = 0.174$, for which maximum $N_2 \approx 35$ (for $Q_{w2} \to \infty$, $N_2 \approx 50$).

To compute the transient waveform in the circuit-equivalent of Fig. 2, we model the secondary line as a chain of $n = 1, 2, \ldots, N_2$ coupled cavities, with cell voltage V_n,[4]

$$\left(\frac{\partial^2}{\partial t^2}+\frac{\omega_n}{Q_n}\frac{\partial}{\partial t}+\omega_n^2\right)V_n=\frac{1}{2}\omega_n^2\left(\kappa_{n-1/2}V_{n-1}+\kappa_{n+1/2}V_{n+1}\right)+2\frac{\omega_1}{Q_{e1}}\frac{\partial V_F}{\partial t}\delta_{n,1}-2k_l\frac{\partial I_n}{\partial t}. \qquad (7)$$

The discharging primary waveform is V_F, the reverse waveform $V_R=V_1-V_F$, and $\delta_{n,1}$ is the Kronecker delta function. Beam-loading is governed by the beam current I_n and the loss-factor $k_l=\omega[R/Q]/4$. The Q of each cell is determined by the wall Q, and, for the end-cells, n=1, N, external coupling quantified by an external Q parameter Q_{en}. To determine the desired values for circuit parameters we analyze Eq. (7) in the frequency domain, with no beam-drive. Interior cell resonance frequencies and coupling constants are determined from the desired operating frequency, phase-shift per cell and the local group velocity. Matching conditions and the line propagation characteristic then determine the end-cell parameters. To solve the system numerically, we express cell voltages as $V_n=\Re\tilde{V}_n(t)e^{j\omega t}$, and employ the slowly-varying envelope approximation. Forward, reverse and first-cell voltages are illustrated in Fig. 3. Note that transient charging causes an overgradient in the early cells $G_{\max}\approx 1.30\,G$ where G is the gradient determined from the steady-state transmission line scalings and is equal to the gradient after N_2 periods.

To illustrate the scalings we consider a numerical example with $N_1=25$ and a gradient of $G\approx 1.01\,\text{GeV/m}$ ($G_{\max}\approx 1.3\,\text{GeV/m}$). The voltage in the first cell is $V_{NL}\approx 1.2\times 10^6\,\text{V}$ and $U_2=V_{NL}^2/4k_l\approx 11.9\text{ mJ}$. The maximum ("hot-spot") power dissipation is $2.3\times 10^{11}\text{ W/m}^2$, and the pulsed temperature rise $\Delta T\approx 126\text{ K}$ is determined from Eq. (3) by the choice of $T_p\approx 0.33\,\text{ns}$. For a 120 Hz machine repetition rate, the duty cycle is 4×10^{-8}, and time-averaged power dissipation is less than $1\,\text{W/cm}^2$. The peak power required from the discharging primary cell is determined by the product of the initial group velocity and energy density in the secondary, $U_2/w_2\approx 5.1\text{J/m}$, and is $U_1/T_p\approx 2.7\times 10^2\,\text{MW}$. The stored energy requirement in one primary cell is then $U_1\approx 88\text{ mJ}$, and the stored energy density in the primary line prior to discharge is $U_1/L\approx 72\text{ J/m}$. For a primary cavity with $\beta\approx 1$ and $\tau_1\approx 1.07$, the pulsed temperature rise is the same and the power required is from Eq. (1) $P_1\approx 2.9\times 10^2\text{ MW}$ in a $\tau_1 T_1\approx 18.6\text{ ns}$

pulse. With these choices, the efficiency of transfer of energy from the primary input to the secondary cells is 40%. (If one accepts as a cyclic fatigue constraint $\Delta T \approx 40$ K, then $G \approx 0.56$ GeV/m with $P_1 \approx 92$ MW and $U_1 / L \approx 23$ J/m)

To appreciate the effects of losses, tapering and beam-loading, results from Eq. (5) are illustrated in Fig. 4, for maximum cell voltages up to $n = 50$ and various conditions. For the lossless case our analytic work predicts that the peak voltage will droop to unity in 50 periods, and this agrees with the result shown in Fig. 4. For the lossy constant-impedance example seen in Fig. 4, the output voltage is reduced to 0.8, consistent with the 2 dB insertion loss one would expect from the steady-state scalings. For the case of attenuation in a constant-gradient structure, peak voltage is 100% at n=33, and 98% at n=35, agreeing with Eq. (6) to 2%. To quantify beam-loading we observe that excitation by a charge q_b amounts to a displacement of the cavity phasor referred to beam-phase, $\tilde{V}_n \rightarrow \tilde{V}_n - 2k_l q_b$, at the time of bunch passage. To illustrate, we time $N_2 = 50$ bunches with $q_b \approx 60$ pC to arrive at the maximum in cell voltage, and phased for maximum acceleration. Voltage droop due to beam-loading is then 5% at n=35 as seen in Fig. 4; this is about 1/3 of the simplest estimate, $2k_l n q_b$, and illustrates a novel feature of beam-loading in this inherently transient device. In a conventional collinear structure each bunch must propagate through the wakefield left by preceding bunches; here, the beam-induced wakefield disperses and its effect on other bunches is thereby diminished.

Having analyzed the ideal behavior, let us consider errors. For random errors in cell resonant frequency, with root-mean-square (rms) $\omega\sigma_\omega$ one has a phase-error at the last cell given by $\delta\varphi \approx \sigma_\omega N_2^{1/2} / \beta_g$. To hold voltage ($\cos\varphi$) error to 1%, $\sigma_\omega < 0.2 / N_c N_2^{1/6} \approx 3 \times 10^{-3}$ (0.27 GHz) for $N_c \approx 30$ and $N_2 \approx 50$. In the case of a uniform error in tune one has $\sigma_\omega < 0.2 / N_c N_2^{2/3} \approx 5 \times 10^{-4}$. To relate σ_ω to dimensional tolerances, we employ a finite-difference code to the geometry of Fig. 2. The actual geometry employed is seen in Fig. 5, in the form of a seven-cell test-structure (matched to standard waveguide, WR10, with a voltage standing wave ratio under 1.1 over 1.6 GHz). In this geometry $[R/Q] \approx 144\ \Omega$, and $Q_w \approx 2.3 \times 10^3$, at 3π/2 phase-advance per cell, and

$\beta_g \approx -0.24$. With this geometry we have surveyed single errors in each of the major cell dimensions and find maximum sensitivity of 0.27 GHz/13 μm corresponding to errors in cell-period or iris gap. At this level conventional machining would be adequate; however, with multiple errors, and lower β_g one approaches the state of the art in precision electro-discharge machining. Sensitivity to bonding was assessed with a 164 μm gap inserted between the coupling irises and the roof and floor. This shifted the mode frequency by -2.1%, and raised the $[R/Q]$ by to $165\,\Omega$, and the wall Q to 2.7×10^3. To assess the effect of filleting, a $127\mu\text{m}\times127\mu\text{m}$ vertical post was placed in the corner of one cell. This raised the mode frequency by 0.5%, with negligible effect on $[R/Q]$, and wall Q. We conclude that filleting and bonding must be accounted for in a final design.

The switch is a critical element in the concept, and, as seen in Fig. 2, we implement this as an H-plane tee in WR10, with a layer of photoconductor placed in port #3, the vertical stub. We are interested in diamond for the photoconductor due to (1) dielectric strength of 1 GV/m, on a μs time scale,[8] (2) high thermal conductivity $\kappa \approx 1.5-2.0\times10^3$ W/K $-$ m,[9] and (3) low loss-tangent $\tan\delta < 5\times10^{-4}$.[10] The effective mobility of electrons and holes in diamond drops quickly for carrier densities greater than $n_e \approx 10^{16}$ cm^{-3},[11] and at this value, the conductivity in diamond is about 6.4×10^2 mho/m, so that skin-depth $\delta \approx 66$ μm. The bandgap is $\varepsilon \approx 5.5\,\text{eV}\,(220\,\text{nm})$ and with uv absorption coefficient well in excess of 10^2 cm^{-1} the required laser fluence is less than 0.1 mJ/cm^2. The carrier lifetime value of 1 ns noted in [11] for synthetic diamond is adequate for our purposes. With stub width $W = 0.12"$ in x and width $b = 0.05"$ along the electric field (as for WR10), the cross-section of the diamond layer is $3.9\times10^{-2}\,\text{cm}^2$, and for a depth of 66 μm, the volume of diamond is $V = 2.6\times10^{-4}\,\text{cm}^{-3}$. At a laser fluence of 0.1 mJ/cm^2, the required laser pulse energy to activate one switch is less than 5 μJ.

Microwave analysis of the switch follows previous work.[12] The 3×3 S-matrix is characterized by two parameters that we calculated with a field-solver, and these determine the required phase-shift through port 3 in the on and off states. These parameters, together with the dielectric constant for diamond $\varepsilon/\varepsilon_0 \approx 5.65$, determine the placement of the shorting plane on the stub, and the peak electric field $E_{\max}$ at the surface of the diamond. We find $E_{\max}(\mathrm{GV/m}) \approx 1.29\sqrt{P_{in}(\mathrm{GW})}$, well below the breakdown threshold of diamond for power levels considered here, and lower than the field in the accelerating cavities. Calculated losses during the on state come to 1.5% or 1.5 mJ for each $0.1\ \mathrm{J}$ discharged. The volume specific heat capacity of diamond is $C \approx 1.81\ \mathrm{J/cm^3\,K}$, corresponding to a heat capacity of $4.7\times10^{-4}\ \mathrm{J/K}$ for the volume V. Pulsed temperature rise in the diamond due to mm-wave losses is under 5 K.

A number of issues are raised by this concept and merit further study. Intrinsic issues are: transverse particle deflections due to the asymmetry of the signal and beam axes, higher multipole content in the fields, cross-talk between secondary lines and performance as a two-dimensional circuit. As to transverse particle deflections, a simple estimate may be obtained by considering the electromagnetic fields as a superposition of TE_{10} mode forward and reverse waves in the unloaded guide, according to which the kick may be compensated by permitting an angle $\theta \approx \beta_g$ deviation from orthogonality. However, a more rigorous treatment remains to be performed to demonstrate a geometry and a mode of operation where the transverse voltage gradient has been zeroed on the beam-axis --- a necessary and sufficient condition for the absence of deflection, according to the Panofksy-Wenzel theorem.

The cell design presented here will benefit from additional refinement in other areas, including cavity-shaping, alternative cavity coupling elements, corner-rounding, and filleting. If mechanical issues permit, significant improvements are possible. Design with a $90°$ transit angle promises a 30% reduction in stored energy. Additional pulse compression may be obtained if it proves possible to relax the single-depth constraint we have accepted. In the limit of a larger primary cavity, with Q and vertical dimension larger by a factor of $O\left(10^1\right)$, one could power a 1-m, 1-GeV, $N_2 \approx 15$ beamline linac with a single power feed providing $4\times10^2\ \mathrm{MW}$ in a $0.2\,\mu\mathrm{s}$ pulse, with stored energy per unit length under $40\ \mathrm{J/m}$. Pulsed temperature rise in the secondary would be under $100\,\mathrm{K}$, and under $40\,\mathrm{K}$ in the primary. For studies at lower power, the same linac could operate at 3-MeV with an existing commericial 5 kW power source, 3 orders of magnitude lower peak power than a conventional linac for the same beam energy. The challenge of designing such a primary cavity lies in the problem of good coupling to the secondary line, so as to maintain a short discharge time-scale, equivalent to an external Q after switch closure of $Q_e \approx 10^2$.

While fundamental concerns remain as to the ultimate gradient "in copper", we have shown that the limits derived for passive structures are not in themselves fundamental, and one can do better, by orders of magnitude.

We thank Angie Seymour for her support. Work was supported by U.S. Department of Energy, Contract DE-AC03-76SF00515.

[1] *Proceedings of the 1996 DPB/DPFWorkshop on New Directions for High Energy Physics* (AIP, New York, 1997).

[2] T. Katsouleas, AIP Proc. **398** (AIP, New York, 1997) pp. 175-180.

[3] D. Pritzkau, *et al.*, (IEEE, New York, to be published) and D. Pritzkau, ARDB-SLAC Technical Note No. 31, 6 September 1996 (unpublished).

[4] D. H. Whittum, *Proceedings of the Joint US-CERN-Japan School, RF Engineering for Particle Accelerators*, (IOP, to be published), SLAC-PUB-7802.

[5] W.W. Hansen, *J. Appl. Phys.* **9** (1938) pp. 654-663.

[6] E. L. Ginzton, W. W. Hansen, and W. R. Kennedy, *Rev. Sci. Instrum.* **19** (1948) pp. 89-108; M. Chodorow, *et al.*, *Rev. Sci. Instrum.* **26** (1955) pp. 134-204.

[7] *The Stanford Two-Mile Accelerator*, R.B. Neal, editor (W.A. Benjamin, New York, 1968).

[8] *Diamond: Electronic Properties and Applications*, L.S. Pan and D.R. Kania, eds. (Kluwer, Boston, 1995) p. 254.

[9] *Handbook of Industrial Diamonds and Diamond Thin Films*, M. A. Prelas, G. Popovici, and L. K. Bigelow, eds. (Marcel Dekker, New York, 1998) pp. 147-192.

[10] M. Thumm, *International Journal of Infrared and Millimeter Waves*, **19** (1998) pp. 3-14.

[11] L. S. Pan, *et al.*, Materials Research Society Symposium, Vol. 302 (1993) pp. 299-304.

[12] S. G. Tantawi, *et al.*, *Advanced Accelerator Concepts*, AIP Proc. **398** (AIP, New York, 1997) pp. 813-821.

FIGURE 1. Accelerator circuit **(a)** during charge-up and **(b)** after switching.

FIGURE 2. Illustrating the geometry of a single period.

FIGURE 3. Illustrating the forward voltage employed for the coupled-cavity simulations, and typical waveforms for the reverse and the input coupler cell voltages

FIGURE 4. This plot illustrates the maximum (over time) of each cell voltage for: a lossless structure. ($Q_w \approx \infty$); a constant-impedance (CZ) line with $Q_w \approx 2700$; a constant-gradient (CG) line with $Q_w \approx 2700$. The dashed curve corresponds to the constant-gradient line with beam-loading.

FIGURE 5. Accelerator matched to standard waveguide.

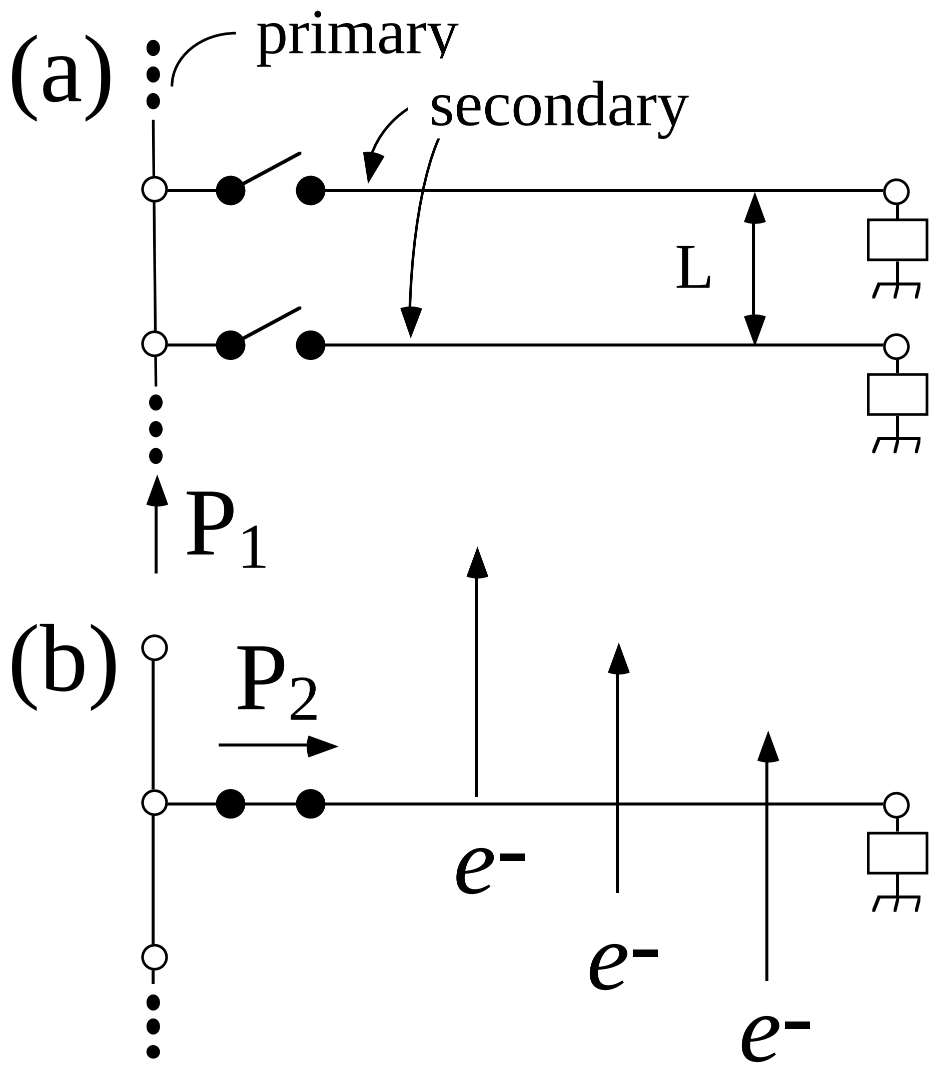

FIG. 1

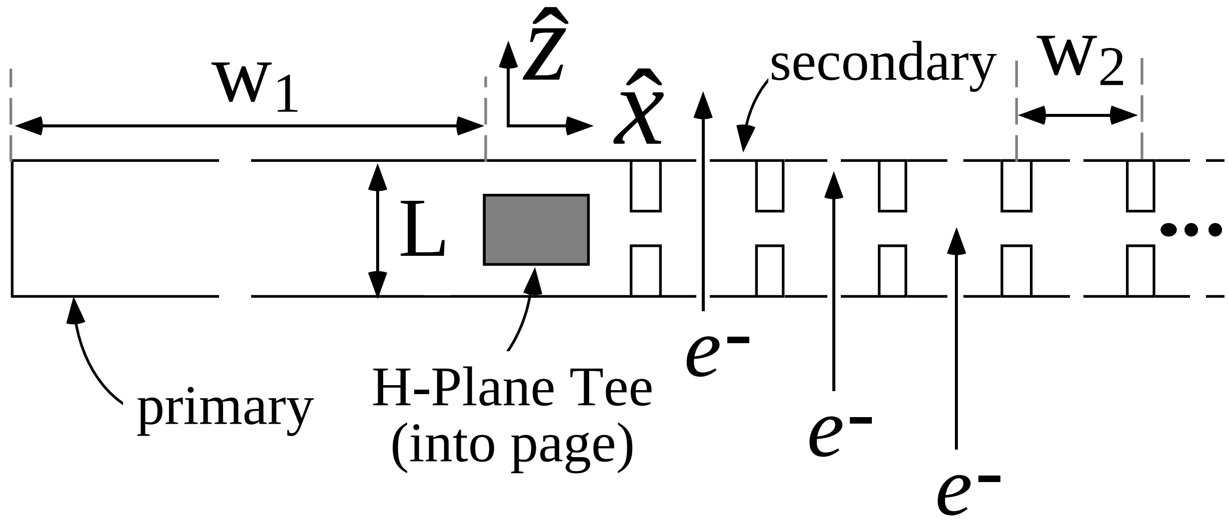
w1
ẑ
x̂
secondary
w2
L
e-
e-
e-
primary
H-Plane Tee
(into page)

FIG. 2

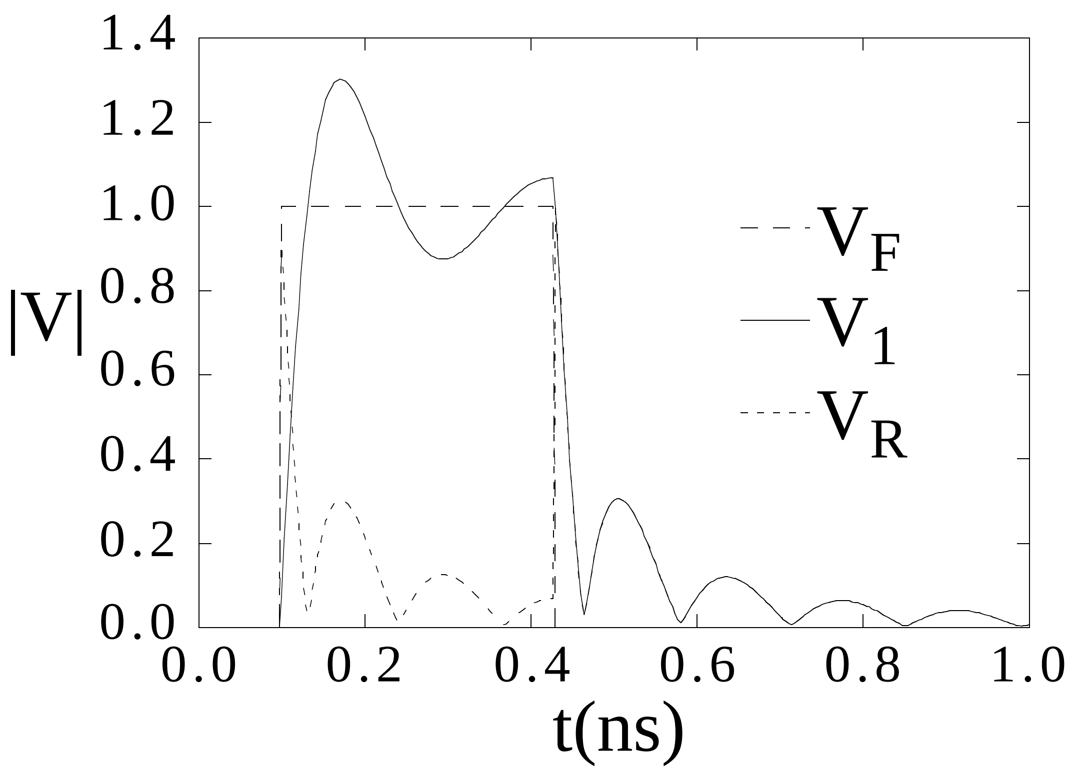
1.4
1.2
1.0
0.8
0.6
0.4
0.2
0.0
|V|
V_F
V_1
V_R
0.0
0.2
0.4
0.6
0.8
1.0
t(ns)

FIG. 3

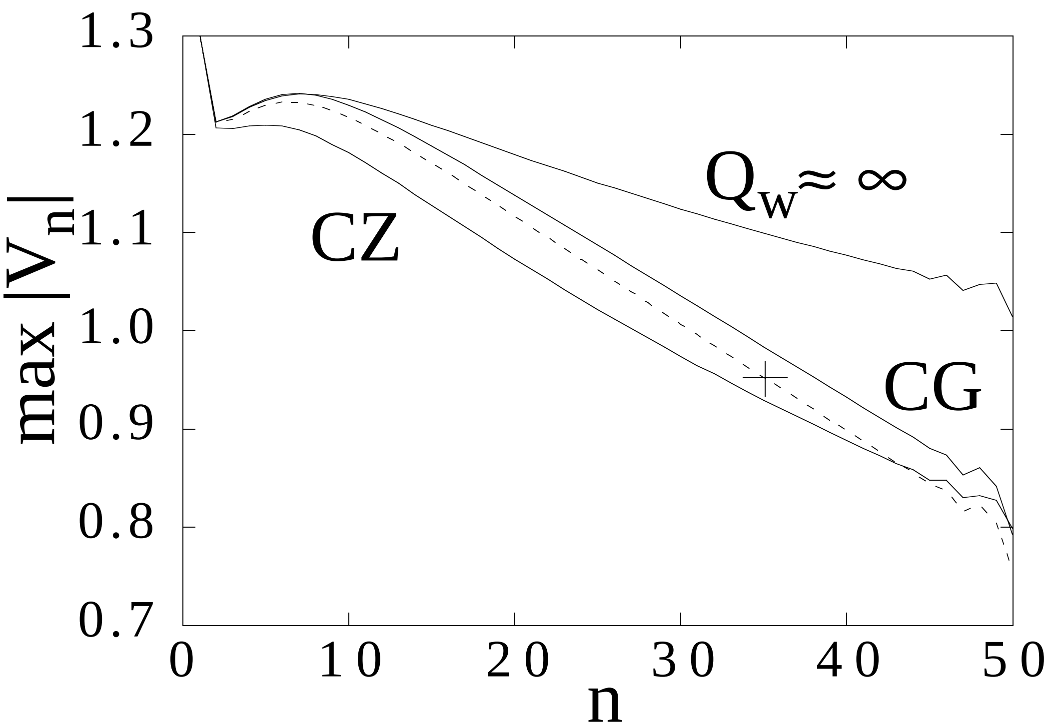

FIG. 4

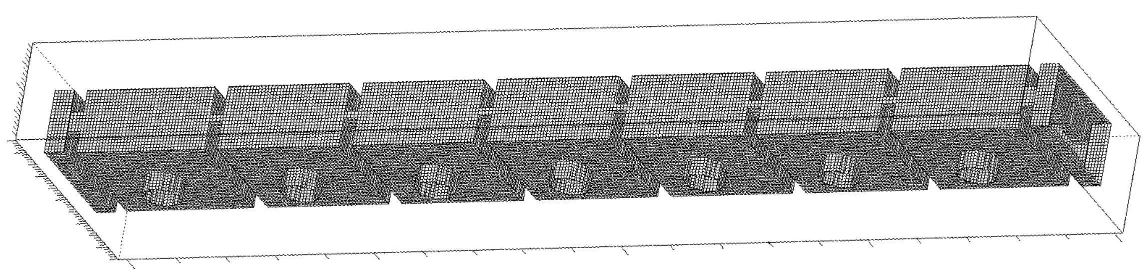

FIG. 5